

Evaluation of a regional air quality model using satellite column NO₂: treatment of observation errors and model boundary conditions and emissions

R. J. Pope¹, M. P. Chipperfield¹, N. H. Savage², C. Ordóñez², L. S. Neal², L. A. Lee¹, S. S. Dhomse¹, and N. A. D. Richards¹

¹School of Earth and Environment, University of Leeds LS2 9JT, Leeds, UK

²Met Office, Exeter, UK

Correspondence to: R. Pope (eerjp@leeds.ac.uk)

Abstract

We compare tropospheric column NO_2 between the UK Met Office operational Air Quality in the Unified Model (AQUM) and satellite observations from the Ozone Monitoring Instrument (OMI) for 2006. Column NO_2 retrievals from satellite instruments are prone to large uncertainty from random, systematic and smoothing errors. We present an algorithm to reduce the random error of time-averaged observations, once smoothing errors have been removed with application of satellite averaging kernels to the model data. This reduces the total error in seasonal mean columns by 30–70 %, which allows critical evaluation of the model. The standard AQUM configuration evaluated here uses chemical lateral boundary conditions (LBCs) from the GEMS (Global and regional Earth-system Monitoring using Satellite and in-situ data) reanalysis. In summer the standard AQUM overestimates column NO_2 in northern England and Scotland, but underestimates it over continental Europe. In winter, the model overestimates column NO_2 across the domain. We show that missing heterogeneous hydrolysis of N_2O_5 in AQUM is a significant sink of column NO_2 and that the introduction of this process corrects some of the winter biases. The sensitivity of AQUM summer column NO_2 to different chemical LBCs and NO_x emissions datasets are investigated. Using Monitoring Atmospheric Composition and Climate (MACC) LBCs increases AQUM O_3 concentrations compared with the default GEMS LBCs. This enhances the NO_x - O_3 coupling leading to increased AQUM column NO_2 in both summer and winter degrading the comparisons with OMI. Sensitivity experiments suggest that the cause of the remaining northern England and Scotland summer column NO_2 overestimation is the representation of point source (power station) emissions in the model.

1 Introduction

Air quality has a major influence on the UK both socially and economically. It can result in approximately 50 000 premature deaths per year and an average reduction in life expectancy of 7–8 months (HoC, 2010). Air pollution health effects include lung disease and

cancer, cardiovascular problems, asthma and eye irritation (WHO, 2011). In 2005, poor UK air quality cost £ (€) 8.5 (10.7)–20.2 (25.5) billion and between 2007–2008 there were 74 000 asthma-related hospital admissions. Overall, these air quality-asthma incidents cost society £ (€) 2.3 (2.9) billion (HoC, 2010). Poor air quality associated with ozone concentrations over 40 ppbv can also significantly reduce crop yields e.g. Hollaway et al. (2012).

Therefore, regional models have been developed to predict hazardous levels of air pollution to help inform the public and to allow local authorities to take action to reduce/accommodate the respective health risks/effects. Air quality models have mainly been evaluated against surface observations, e.g. Savage et al. (2013). Recently such models have also been compared with satellite observations, taking advantage of the better spatial coverage despite the potentially large error of individual observations. In the past NO₂ satellite data has been compared mainly with global atmospheric chemistry models (e.g. Velders et al., 2001; Lauer et al., 2002; Van Noije et al., 2006). More recently, other studies have used satellite data to evaluate models on a regional scale. Savage et al. (2008) investigated European tropospheric column NO₂ interannual variability (IAV) during 1996–2000 by comparing GOME with the TOMCAT chemical transport model (CTM) (Monks et al., 2012). The best comparisons were found in the JFM and AMJ seasons, especially over western Europe. They also found that synoptic meteorology had more influence on NO₂ IAV than NO_x emissions did.

Huijnen et al. (2010) compared Ozone Monitoring Instrument (OMI) tropospheric column NO₂ against a European global-regional air quality model ensemble median for 2008–2009. The ensemble compared better with the OMI data than any individual model, with good agreement over the urban hotspots. Overall, the spread in the models was greatest in the summer (with deviations from the mean OMI tropospheric column in the range 40–62 %), due to the more active NO_x chemistry in this season and the differences in chemistry schemes among the contributing models, when compared to winter (20–34 %). Several of the regional models successfully simulated the shipping lanes seen by OMI.

Han et al. (2011) investigated tropospheric column NO₂ over the Korean Peninsula through comparisons between OMI data and the Community Multi-scale Air Quality Model

(CMAQ) (Foley et al., 2010). In summer, North and South Korea had similar column NO_2 from both the model and observations. In winter, South Korea, a more developed nation with greater infrastructure, had significantly greater NO_2 concentrations than North Korea. Overall, CMAQ overestimated OMI NO_2 concentrations by factors of 1.38–1.87 and 1.55–7.46 over South and North Korea, respectively.

Other studies investigating regional tropospheric column NO_2 through model simulations and satellite observations include Blond et al. (2007), Boersma et al. (2009) and Curier et al. (2014). Blond et al. (2007) compared CHIMERE 3-D CTM and SCIAMACHY column NO_2 over western Europe; they found reasonable agreement with winter and summer correlations of 0.79 and 0.82, respectively. Boersma et al. (2009) used the GEOS-Chem 3-D CTM to explain the seasonal cycle in SCIAMACHY and OMI column NO_2 over Israeli cities, with larger photochemical loss of NO_2 in summer than winter. Curier et al. (2014) used a combination of OMI and the LOTOS-EUROS 3-D CTM to evaluate NO_x trends finding negative trends of 5–6 % per year over western Europe.

The UK Met Office's Air Quality in the Unified Model (AQUM) is used for short operational chemical weather forecasts of UK air quality. Savage et al. (2013) performed the first evaluation of the AQUM operational forecast for the period May 2010–April 2011 by using surface O_3 , NO_2 and particulate matter observations from the UK Automated Urban and Rural Network (AURN) (DEFRA, 2012). Among other model-observation metrics they used the mean bias (MB), root mean square error (RMSE), modified normalised mean bias (MNMB) and the Fractional Gross Error (FGE) (Seigneur et al., 2000). See the Appendix for the definition of these metrics.

Savage et al. (2013) found that AQUM overestimated O_3 by $8.38 \mu\text{g m}^{-3}$ (MNMB = 0.12), with a positive bias at urban sites but no systematic bias at rural sites. The model-observation correlation was reasonably high at 0.68. For NO_2 , there was a bias of $-6.10 \mu\text{g m}^{-3}$, correlation of 0.57 and MNMB of -0.26 . At urban sites there was a large negative bias while rural sites had marginal positive biases. The coarse resolution of AQUM (12 km) led to an underestimation at urban sites because the model NO_x emissions are in-

stantaneously spread over the entire grid box. The particulate matter (PM_{10}) prediction skill was lower with a correlation and bias of 0.52 and $-9.17 \mu\text{g m}^{-3}$, respectively.

The aim of this paper is to evaluate AQUM using satellite atmospheric trace gas observations. The Met Office has previously compared the skill of AQUM only against AURN surface measurements, which in the case of NO_2 are not specific and include contributions from other oxidised nitrogen compounds (see Savage et al. (2013), and references therein). Therefore, for better spatial model-observation comparisons and to minimise the effect of measurement interferences, we use satellite observations over the UK. We focus on tropospheric column NO_2 data from OMI for the summer (April–September) and winter (January–March, October–December) periods of 2006. Section 2 describes the OMI satellite data used and gives a detailed account of our error analysis which determines how we can use satellite data to test AQUM. Section 3 describes AQUM and the model experiments performed. Results from the model-observations comparisons are given in Sect. 4. Section 5 presents our conclusions.

2 Satellite data

OMI is aboard NASA's EOS-Aura satellite and has an approximate London daytime overpass at 13:00 LT. It is a nadir-viewing instrument with a pixel size of 312 km^2 and 3240 km^2 along track and across track, respectively (Boersma et al., 2008). We have taken the DOMINO tropospheric column NO_2 product, version 2.0, from the TEMIS (Tropospheric Emissions Monitoring Internet Service) website, <http://www.temis.nl/airpollution/no2.html> (Boersma et al., 2011b, a). We have binned NO_2 swath data from 1 January to 31 December 2006 onto a daily 13:00 LT $0.25^\circ \times 0.25^\circ$ grid between $43\text{--}63^\circ \text{ N}$ and $20^\circ \text{ W--}20^\circ \text{ E}$. All satellite retrievals have been quality controlled, and retrievals/pixels with geometric cloud cover greater than 20 % and poor quality data flags (flag = -1) were removed. The product uses the algorithm of Braak (2010) to identify OMI pixels affected by row anomalies and sets the data flags to -1 . Therefore, indirectly, we are filtering out the OMI row anomalies as well, even though this effect was limited in 2006. OMI has an approximate 13:00 LT Lon-

don overpass, but we used all OMI retrievals in the domain between 11:00 and 15:00 LT to get more extensive spatial coverage. Several studies have validated OMI column NO₂ against surface and aircraft measurements of tropospheric column NO₂. Irie et al. (2012) compared SCIAMACHY, OMI and GOME-2 tropospheric column NO₂ with surface MAX-DOAS column NO₂ observations between 2006 and 2011. They found the instruments are biased by $-5 \pm 14\%$, $-10 \pm 14\%$, and $+1 \pm 14\%$, respectively, which the authors suggest are all small and insignificant. Boersma et al. (2008) compared the near real time (NRT) OMI product (version 0.8) with aircraft measurements in the INTEx-B campaign. Overall, they found a good correlation (0.69) between OMI and the aircraft column NO₂, with no significant biases. Therefore, we have confidence in the OMI column NO₂ and use it for evaluation of our model.

2.1 Satellite averaging kernels

Model transfer functions (MTF), known as "averaging kernels (AK)", allow for direct comparison between model column NO₂ and satellite retrievals. This section introduces how these MTF (AK) modify model vertical profiles and how they vary in season and location. Eskes and Boersma (2003) define the AK to be a relationship between the retrieved quantities and the true distribution of the tracer (i.e. the vertical profile of a chemical species). In other words, the satellite instrument's capability to retrieve a quantity is a function of altitude. For instance, the instrument may be more or less sensitive retrieving a chemical species near the boundary layer than in the stratosphere. Therefore, since satellite retrievals and model vertical profiles are not directly comparable, the AK (or weighting function) is applied to the model data, so the sensitivity of the satellite is accounted for in the comparisons. The AK comes in different forms for different retrieval methods. For the Differential Optical Absorption Spectroscopy (DOAS) method, the AK is in the form of a column vector, while in Optimal Estimation, the AK is a matrix whose dimensions depend on the number of pressure levels in the retrieval process.

The OMI retrievals use the DOAS technique and the AK is a column vector. Following Huijnen et al. (2010) and the OMI documentation (Boersma et al., 2011a), the AKs are

applied to the model as:

$$y = \mathbf{A} \cdot \mathbf{x} \quad (1)$$

where y is the total column, \mathbf{A} is the AK and \mathbf{x} is the vertical model profile. However, here the tropospheric column is needed:

$$y_{\text{trop}} = \mathbf{A}_{\text{trop}} \cdot \mathbf{x}_{\text{trop}} \quad (2)$$

where \mathbf{A}_{trop} is:

$$\mathbf{A}_{\text{trop}} = \mathbf{A} \cdot \frac{\text{AMF}}{\text{AMF}_{\text{trop}}} \quad (3)$$

AMF is the atmospheric air mass factor and AMF_{trop} is the tropospheric air mass factor. For the OMI product, Huijnen et al. (2010) state the AK tends to be lower than 1 in the lower troposphere (e.g. 0.2–0.7 up to 800 hPa) and greater than 1 in the mid-upper troposphere. Therefore, the OMI AKs reduce model NO_2 subcolumns in the lower troposphere and increase them in the mid-upper troposphere (Huijnen et al., 2010). Figure 1 shows example tropospheric AKs for summer and winter profiles over London (urban – higher column NO_2) and Dartmoor (rural area in southwest England – lower column NO_2), which have been coloured by their respective tropospheric AMFs. In the lower troposphere for both seasons and locations the tropospheric AKs range around 0–1. However, in the mid-upper troposphere, the London tropospheric AKs tend to be greater than Dartmoor in both seasons. London tropospheric AKs are most pronounced in winter, with some tropospheric AKs over 8, while in the summer they range around 1–8. In both seasons, the tropospheric AMFs are biggest, 5–6, in the lower range tropospheric AKs, 0–1, and smaller, 0–1.5 as the tropospheric AKs range increases, over 2. If the tropospheric AMFs are small (i.e. near 0 suggesting the majority of the NO_2 is within the lower layers of the London boundary layer; also small tropospheric AKs there), from Eq. (3), as the full atmospheric AKs naturally increase with altitude, the tropospheric AMFs will return larger tropospheric AKs. Also,

in winter over London, the shallower boundary layer will trap larger winter emissions of NO₂ closer to the surface. Therefore, the tropospheric AMF will be smaller and the winter mid-upper tropospheric AKs will be larger as seen in Fig. 1. Over Dartmoor, the AKs show less seasonal variation and the majority range around 1–6 for both summer and winter. This is also seen in the tropospheric AMF, which ranges around approximately 0–6, but has no clear pattern in the Dartmoor tropospheric AKs, in both seasons.

The Dartmoor AKs tend to be lower than those of London, which could be a result of multiple factors: surface albedo, viewing geometry, cloud cover, etc. As data with cloud cover higher than 20% is filtered out and the viewing geometry of London and Dartmoor will vary depending on where OMI is in its orbit (both locations are at similar latitudes), we suggest that neither is the dominant cause of the AK differences. The surface albedo data in the satellite files is noisy and shows no clear pictures between London and Dartmoor. We suggest that the different NO₂ loading between the locations is the primary factor in the AK differences. Eskes and Boersma (2003) state that AKs are independent of trace gas distributions for optically thin absorbers. However, for stronger absorbers they suggest that the AK depends on the true distribution of the tracer. Therefore, as London column NO₂ is greater than that of Dartmoor, i.e. regions of optically strong and thin absorbers, the AKs are more and less sensitive, respectively.

2.2 Differential optical absorption spectroscopy NO₂ retrieval error

The DOAS retrievals are subject to random, systematic and smoothing errors in the retrieval process. Random (quasi-systematic) errors include fitting errors, cloud errors, instrument noise and signal corruption. Systematic errors include absorption cross-sections, surface albedo and stratospheric correction uncertainties. Finally, smoothing errors include biases in the a priori profiles and sensitivity of the satellite when recording the slant column through the atmosphere. If multiple retrievals are averaged together, as in this study, the random errors will partially cancel leading to the random error being reduced by a factor of $\frac{1}{\sqrt{N}}$ (where N is the number of retrievals).

In contrast, systematic errors are unaffected by cancelling through averaging. In the following section we investigate the different error components of the satellite retrievals and derive an expression for the error in the averaged retrievals. This methodology should give smaller errors which are more representative of the time-averaged retrieval error and so allow a stricter test of the model. Boersma et al. (2004) describe the error in the DOAS NO₂ retrievals as:

$$\sigma_{\text{trop}}^2 = \left(\frac{\sigma_{\text{total}}}{\text{AMF}_{\text{trop}}} \right)^2 + \left(\frac{\sigma_{\text{strat}}}{\text{AMF}_{\text{trop}}} \right)^2 + \left(\frac{(X_{\text{total}} - X_{\text{strat}}) \sigma_{\text{AMF}_{\text{trop}}}}{\text{AMF}_{\text{trop}}^2} \right)^2 \quad (4)$$

where σ_{trop} , σ_{strat} and σ_{total} are the uncertainties in the tropospheric vertical, stratospheric slant and total slant columns, respectively. AMF_{trop} is the tropospheric air mass factor, $\sigma_{\text{AMF}_{\text{trop}}}$ is the error in the tropospheric air mass factor, X_{total} is the total slant column and X_{strat} is the stratospheric slant column.

σ_{total} is made up of both random and systematic error, where the random error component can be reduced by $\frac{1}{\sqrt{N}}$. The sources of systematic error in the total slant column include the NO₂ cross-section, spectral calibration, solar diffuser and temperature (Boersma et al., 2004). We assume that the systematic and random errors can be combined in quadrature. In Eq. (6) there are two terms for σ_{total} ; $\sigma_{\text{total,ran}}$ and $\sigma_{\text{total,sys}}$, which are the random and systematic error components of the total slant column, respectively. Boersma et al. (2004) state that $\sigma_{\text{total,sys}}$ can be expressed as $\sigma_{\text{total,sys}} = 0.03 X_{\text{total}}$. We treat σ_{strat} here as systematic as both the OMI standard and DOMINO products estimate the stratospheric slant column using TM4 chemistry-transport model simulations and data assimilation (Dirksen et al., 2011). According to the DOMINO OMI product documentation (which references Boersma et al., 2004, 2007; Dirksen et al. (2011)), the error in the stratospheric slant column is estimated to be 0.25×10^{15} molecules cm⁻² in all cases. However, according to Belmonte Rivas et al. (2014), the stratospheric slant column error does not propagate into the tropospheric column error as it is absorbed by the stratospheric assimilation procedure. Therefore, the σ_{strat} term is removed from Eq. (4).

Boersma et al. (2004) state that the tropospheric column is calculated as:

$$N_{\text{trop}} = \frac{X_{\text{total}} - X_{\text{strat}}}{\text{AMF}_{\text{trop}}} \quad (5)$$

where N_{trop} is the vertical tropospheric column and can be substituted, including the σ_{total} estimates, into Eq. (4). This leads to:

$$5 \quad \sigma_{\text{trop}}^2 = \left(\frac{\sigma_{\text{totalran}}}{\text{AMF}_{\text{trop}}} \right)^2 + \left(\frac{0.03X_{\text{total}}}{\text{AMF}_{\text{trop}}} \right)^2 + \left(\frac{N_{\text{trop}}\sigma_{\text{AMF}_{\text{trop}}}}{\text{AMF}_{\text{trop}}} \right)^2 \quad (6)$$

σ_{trop} is reduced in the model-satellite comparisons when the AK is applied to the model data. Therefore, the error product, $\sigma_{\text{trop}_{\text{ak}}}$, from the OMI retrieval files with the smoothing error removed is used instead of σ_{trop} in Eqs. (4) and (6).

Boersma et al. (2007) suggest that the uncertainty in the tropospheric AMF is around 10–
10 40 %. Therefore, we take the conservative estimate of $\sigma_{\text{AMF}_{\text{trop}}} = 0.4 \cdot \text{AMF}_{\text{trop}}$. This leads to the new retrieval error approximation of:

$$\sigma_{\text{trop}_{\text{ak}}}^2 = \left(\frac{\sigma_{\text{totalran}}}{\text{AMF}_{\text{trop}}} \right)^2 + \left(\frac{0.03X_{\text{total}}}{\text{AMF}_{\text{trop}}} \right)^2 + (0.4N_{\text{trop}})^2 \quad (7)$$

All of these terms are known apart from σ_{totalran} . We can rearrange to calculate this based on other variables provided in the OMI product files. This leads to:

$$15 \quad \left(\frac{\sigma_{\text{totalran}}}{\text{AMF}_{\text{trop}}} \right)^2 = \sigma_{\text{trop}_{\text{ak}}}^2 - (0.4N_{\text{trop}})^2 - \left(\frac{0.03X_{\text{total}}}{\text{AMF}_{\text{trop}}} \right)^2 \quad (8)$$

In the rare case that the right hand side is negative (e.g. when N_{trop} is large, but has small uncertainty; X_{total} is scaled by 0.03 so will be small compared to N_{trop}), the random error component cannot be found as it would be complex, so the random error component is then set to 50 % (H. Eskes, personal communication, 2012). Now, rearranging for σ_{totalran} ,

and assuming the right hand side is positive, Eq. (8) becomes:

$$\sigma_{\text{totalran}} = \text{AMF}_{\text{trop}} \sqrt{\left(\sigma_{\text{tropak}}^2\right) - (0.4N_{\text{trop}})^2 - \left(\frac{0.03X_{\text{total}}}{\text{AMF}_{\text{trop}}}\right)^2} \quad (9)$$

This quantity was calculated for each retrieval in each grid square and then the new seasonal retrieval error was calculated taking the reduced random component into account:

$$\overline{\sigma_{\text{tropak}}} = \sqrt{\left(\frac{\overline{\sigma_{\text{totalran}}}}{\sqrt{N\text{AMF}_{\text{trop}}}}\right)^2 + \left(\frac{0.03\overline{X_{\text{total}}}}{\text{AMF}_{\text{trop}}}\right)^2 + (0.4\overline{N_{\text{trop}}})^2} \quad (10)$$

where a bar superscript represents the seasonal time average.

Figure 2 shows how averaging, by decreasing the random error component, reduces the seasonal satellite tropospheric column error as calculated by our algorithm. The figure compares the simple mean of the total satellite column NO₂ error (calculated for each pixel) with our new method which reduces the estimated random error component by one over the square root of the number of observations. The reduction in the satellite column error is then presented as a percentage of the original satellite column seasonal mean error. In both summer and winter, the seasonal mean column error is reduced to 30–90 % across the domain, therefore making the OMI data much more useful for model evaluation. Table 1 gives examples of the seasonal tropospheric column NO₂ error and the reduced tropospheric column NO₂ error using our algorithm for multiple locations across Europe. The error in summer, compared with winter, and the error over sea in comparison to land, are smaller. We suggest that the larger sample size in summer and over the sea, when compared to winter and over the land, respectively, reduces the random error component further as N is larger. Only for a few retrievals over Scandinavia, does this methodology of reducing the random error component increase the overall column error (not shown here).

3 Air quality in the unified model (AQUM)

3.1 Model setup

The AQUM domain covers the UK and part of continental Europe on a rotated grid between approximately 45–60° N and 12° W–12° E. The model has a horizontal resolution of 0.11° × 0.11° with 38 vertical levels between the surface and 39 km. The model has a coupled, online tropospheric chemistry scheme using the United Kingdom Chemistry and Aerosols (UKCA) subroutines. The chemistry scheme (Regional Air Quality, RAQ) includes 40 tracers, 23 photolysis reactions and 115 gas-phase reactions (Savage et al., 2013) including the reaction of the nitrate radical with formaldehyde, ethene, ethane, propene, n-butane, acetaldehyde, isoprene, organic nitrates and the hydroperoxyl radical. The standard model setup does not include any heterogeneous chemistry. A complete chemical mechanism is included in the online supplement to Savage et al. (2013).

The model uses the Coupled Large-scale Aerosol Simulator for Studies In Climate (CLASSIC) aerosol scheme. This is a bulk aerosol scheme with the aerosols treated as an external mixture. It contains six prognostic tropospheric aerosol types: ammonium sulphate, mineral dust, fossil fuel black carbon (FFBC), fossil fuel organic carbon (FFOC), biomass burning aerosols and ammonium nitrate. In addition, there is a diagnostic aerosol scheme for sea salt and a fixed climatology of biogenic secondary organic aerosols (BSOA). For more details of the aerosol scheme see Bellouin et al. (2011). In common with most regional air quality forecast models in Europe, AQUM shows a small negative bias for PM_{2.5} and a larger negative bias for PM₁₀. For full details of the performance of the model for aerosols, NO₂ and ozone see Savage et al. (2013).

Meteorological initial conditions and lateral boundary conditions (LBCs) come from the Met Office's operational global Unified Model (25 km × 25 km) forecast. Initial chemical conditions come from the previous day's AQUM forecast and aerosol and chemistry LBCs come from the ECMWF GEMS (Global and regional Earth-system Monitoring using Satellite and in-situ data) reanalysis (Hollingsworth et al., 2008). The GEMS fields, available at <http://>

//www.gmes-atmosphere.eu/, provide boundary fluxes for regional air quality models such as AQUM.

This configuration of AQUM uses emission datasets from the National Atmospheric Emissions Inventory (NAEI) ($1 \text{ km} \times 1 \text{ km}$) for the UK, ENTEC ($5 \text{ km} \times 5 \text{ km}$) for the shipping lanes and European Monitoring and Evaluation Programme (EMEP) ($50 \text{ km} \times 50 \text{ km}$) for the rest of the model domain. Over the UK the NAEI NO_x emissions datasets are made up of two source types: area and point. Area sources include traffic, light industry and urban emissions, while point sources are power stations, landfill, incinerators and refineries. Typically, the point source emissions are 100 g s^{-1} in magnitude, while the area sources tend to be 10 g s^{-1} . For most of the experiments we use 2007 instead of 2006 NO_x sources because the ENTEC shipping emissions ($5 \text{ km} \times 5 \text{ km}$ resolution) are available for this year, while only the coarse EMEP shipping emissions are available for the earlier years (Savage et al., 2013). The difference between 2006 and 2007 point source emissions are negligible in altering the AQUM column NO_2 (not shown). Therefore, we use the 2007 emissions datasets throughout this study. The fractional seasonal cycle, which comes from Visschedijk et al. (2007), applied to AQUM's annual NO_x emissions can be seen in Figure 3.

The lightning emissions are based on a parameterisation linked to the model's convection scheme. For details see O'Connor et al. (2014). We do not have a separate parameterisation for soil NO_x emissions but given the large emissions from transport and industry, the soil NO_x emissions are unlikely to be important in this region.

Poupkou et al. (2010) provide the monthly climatology of biogenic emissions on a $0.125^\circ \times 0.0625^\circ$ resolution. The use of climatological biogenic isoprene emissions will partially diminish AQUM's representation of ozone from biogenic precursors. A new interactive biogenic isoprene scheme is under development but was not available for this study. However, this is a secondary issue in this paper as we focus on primary emissions of NO_x . Biomass burning emissions of aerosols come from the Global Fire Emissions Database (GFED), version 1, (Randerson et al., 2005) for 2000. The use of biomass burning emissions from 2000 is somewhat arbitrary, but within the AQUM's domain these emissions have relatively little impact.

3.2 Sensitivity experiments

We performed one control and five sensitivity experiments to investigate the AQUM's simulation of column NO_2 . Two experiments used different LBCs, two experiments used modified point source emissions and two included heterogeneous chemistry. These are summarised in Table 2.

Simulation MACC investigates the sensitivity of AQUM column NO_2 to different chemical LBCs from the global Monitoring Atmospheric Composition and Climate (MACC) reanalysis, which is the follow-on project of GEMS (Inness et al., 2013). The MACC reanalysis uses a more recent version of the ECMWF model (Integrated Forecast System), assimilates more satellite products and was run at a resolution of 80 km instead of 125 km. Savage et al. (2013) have undertaken a similar analysis of the MACC LBCs in AQUM. They showed that when compared with the AURN observations of O_3 , AQUM-MACC performs well during the first quarter of 2006 and overestimates observations afterwards, while AQUM-GEMS has a negative bias during the first quarter of the year but compares well with observations afterwards.

We have performed additional runs to examine the impact of the point sources over the UK on NO_2 columns. The motivation behind Run E1 was to determine the impact of the NO_x point sources on the simulated column NO_2 budget, as we hypothesised that the AQUM's representation of them was the cause of some of the AQUM-OMI column NO_2 positive biases (see Sect. 4.1). Run E2 introduces a new idealised passive tracer emitted from the UK point sources with the same emissions to that of the model NO_x inventory. The idealised tracer is transported like any chemical tracer, but is not lost through chemical reactions. Instead it is lost through its e-folding lifetime of one day. The point source tracer columns can then be examined to see if they correlate with summer AQUM-OMI positive biases (see Sect. 4.3).

Runs $\text{N}_2\text{O}_5\text{High}$ and $\text{N}_2\text{O}_5\text{Low}$ investigate the impact of heterogeneous chemistry on NO_2 columns. Tropospheric NO_x ($\text{NO} + \text{NO}_2$) sources are dominated by anthropogenic

emissions and the loss of NO_2 to HNO_3 is through two pathways:



The standard configuration of AQUM does not include any heterogeneous reactions such as the hydrolysis of N_2O_5 on aerosol surfaces (see details of the chemistry scheme in the Supplement of Savage et al., 2013). Previous global modelling studies have shown that this process can be a significant NO_x sink at mid-latitudes in winter (e.g. Tie et al., 2003; Macintyre and Evans, 2010). Following those analyses, we have implemented this reaction, with rate k (s^{-1}) calculated as:

$$k = \frac{A\gamma\omega}{4} \quad (11)$$

where A is the aerosol surface area ($\text{cm}^2 \text{cm}^{-3}$), γ is the uptake coefficient of N_2O_5 on aerosols (non-dimensional) and $\omega = 100[8RT/(\pi M)]^{\frac{1}{2}}$ (cm s^{-1}) is the root-mean-square molecular speed of N_2O_5 at temperature T (K), M is the molecular mass of N_2O_5 (kg mol^{-1}) and $R = 8.3145 \text{ J mol}^{-1} \text{ K}^{-1}$.

Macintyre and Evans (2010) investigated the sensitivity of N_2O_5 loss on aerosol by using a range of uptake values (0.0 , 10^{-6} , 10^{-4} , 10^{-3} , 5×10^{-3} , 10^{-2} , 2×10^{-2} , 0.1 , 0.2 , 0.5 and 1.0). They found that limited sensitivity occurs at low and high values of γ . At low values, the uptake pathway is an insignificant route for NO_x loss. At high values, the loss of NO_x through heterogeneous removal of N_2O_5 is limited by the rate of production of NO_3 , rather than the rate of heterogeneous uptake. However, in the northern extra-tropics (including the AQUM domain), their model shows significant sensitivity to intermediate values of γ (0.001 – 0.02) with a significant loss of NO_x . Therefore, we experiment with $\gamma = 0.001$ and 0.02 to investigate the sensitivity of AQUM column NO_2 to heterogeneous chemistry. The aerosol surface area, A , includes the contribution of seven aerosol types present in CLASSIC: sea

salt aerosol, ammonium nitrate, ammonium sulphate, biomass burning aerosol, black carbon, FFOC and BSOA. To account for hygroscopic growth of the aerosols, the formulation of Fitzgerald (1975) is used for growth above the deliquescence point for ammonium sulphate ($RH = 81\%$), sea salt ($RH = 75\%$) and ammonium nitrate ($RH = 61\%$) up to 99.5% RH.

5 We apply a linear fit between the efflorescence ($RH = 30\%$ for sulphate, 42% for sea-salt and 30% for nitrate) and deliquescence points. There is no hygroscopic growth below the efflorescence point. Look-up tables are used for the other aerosol types. Biomass burning and FFOC aerosol growth rates are taken from Magi and Hobbs (2003), BSOA growth rates come from Varutbangkul et al. (2006) and black carbon is considered to be hydrophobic (no growth).

3.3 Statistical comparisons

For the AQUM-satellite comparisons the following model-observation statistics were used: Mean Bias (MB), Root Mean Square Error (RMSE) and the Fractional Gross Error (FGE, bounded by the values 0 to 2). These statistics are described by Han et al. (2011) and Savage et al. (2013). Further details are given in the Appendix.

4 Results

4.1 Control run

Figure 4 compares observed column NO_2 with the AQUM control Run C (with AKs applied). The AQUM and OMI averages have similar spatial patterns, with maximum and minimum column NO_2 over the urban and rural/ocean regions, respectively. In summer, AQUM and OMI background concentrations are around $O(10^{13}) - 3 \times 10^{15}$ molecules cm^{-2} , where $O(10^{13})$ represents values in size of the order of 10^{13} . The OMI peak column NO_2 of $16 - 20 \times 10^{15}$ molecules cm^{-2} is over London. AQUM simulates similar London column NO_2 , but the model peak concentrations are over northern England at over 20×10^{15} molecules cm^{-2} .

In winter, the background column NO_2 is elevated with a larger spatial extent ranging around $0(10^{13})$ – 6×10^{15} molecules cm^{-2} in both the AQUM and OMI fields. However, the elevated AQUM background state has a larger coverage than that of OMI. Over the source regions, OMI column NO_2 peaks over London at 12 – 13×10^{15} molecules cm^{-2} , with similar concentrations seen in AQUM. However, AQUM peak column NO_2 are over northern England at 12 – 16×10^{15} molecules cm^{-2} . Therefore, independently of season, AQUM overestimates northern England column NO_2 . Interestingly, the background column NO_2 is larger in winter for both AQUM and OMI, but column NO_2 is lower over the source regions in winter than in summer (Pope et al., 2014). van der A et al. (2008) suggest that peak UK NO_x emissions occur in July, while Pope et al. (2014) suggest that the transport of column NO_2 away from source regions due to stronger winter dynamics outweighs the loss of UK source region column NO_2 from enhanced summer photochemistry.

Figure 5 shows the MB between AQUM Run C and OMI. The black polygoned regions show significant differences, i.e. where the magnitude of the MB is greater than the satellite error. In summer, there are significant positive, 5 – 10×10^{15} molecules cm^{-2} , and negative, -10 to -1×10^{15} molecules cm^{-2} , biases in northern England and the Benelux region, respectively. The negative biases are potentially linked to the coarser resolution EMEP NO_x emissions datasets ($50 \text{ km} \times 50 \text{ km}$) which average emissions over a larger grid square causing AQUM to simulate lower column NO_2 than seen by OMI. We hypothesise that the northern England biases are linked to the point source (power station) NO_x emissions from NAEI. This is further discussed in Sect. 4.3. In winter, AQUM overestimates OMI by 1 – 3×10^{15} molecules cm^{-2} over the North Sea and Scotland, as the modelled winter background column NO_2 is larger; this is further investigated in Sect. 4.4 by including an additional NO_x sink in the chemistry scheme of the model. The northern England positive biases seen in summer also extend to winter, 3 – 5×10^{15} molecules cm^{-2} , suggesting that this is not only a seasonal feature. Finally, the large bias dipole in the Po Valley appears to be related to the LBCs or the winter emissions, as summer biases are small.

We also compared AQUM against surface observations of NO_2 from AURN, found at <http://uk-air.defra.gov.uk/networks/network-info?view=aurn>, and maintained by DEFRA.

This was to see if there was a consistent pattern in the biases in the model column and surface NO_2 . However, we find similar problems to Savage et al. (2013) where surface AQUM – observation comparisons show systematic negative biases at urban sites. The coarse model resolution, compared to the observation point measurements (even with roadside and traffic sites removed), results in significant model underestimation of NO_2 in urban regions. Therefore, it is difficult to draw any conclusions on the AQUM skill as the model grid-point data will struggle to reproduce the point measurement observations. Also the spatial coverage of the AURN data is very sparse over the UK and AURN NO_2 measurement interferences from molybdenum converters (Steinbacher et al., 2007) overestimate surface concentrations, in particular at rural sites. Therefore, satellite (pixel area) data are the primary observations used to evaluate AQUM in this paper.

4.2 Impact of lateral boundary conditions

Figure 6a and b shows results of the sensitivity run with the MACC boundary conditions (Run MACC) and can be compared with Fig. 4a and b. The MACC LBCs have a limited impact on summer column NO_2 with peak concentrations over London and Northern England between $15\text{--}20 \times 10^{15}$ molecules cm^{-2} for both runs MACC and C. However, in winter Run MACC increases column NO_2 from approximately 12×10^{15} to 16×10^{15} molecules cm^{-2} over the UK and Benelux region. When compared with OMI (Fig. 6c and d) the limited summer impact of the MACC LBCs results in biases which are similar to those in Fig. 5 from the control run, with biases over northern England, $5\text{--}10 \times 10^{15}$ molecules cm^{-2} , and continental Europe, -5 to -3×10^{15} molecules cm^{-2} . In winter, Run MACC has enhanced column NO_2 resulting in biases with OMI of between $2\text{--}5 \times 10^{15}$ molecules cm^{-2} across the whole domain, unlike Run C with GEMS LBCs in Fig. 5. The peak positive biases are again over northern England (and the Po Valley), 5×10^{15} molecules cm^{-2} , suggesting that AQUM overestimates NO_2 in the region, at the OMI overpass time, independently of season or LBCs. Therefore, the GEMS LBCs appear to give better AQUM column NO_2 forecast skill than MACC does, similarly as found by Savage et al. (2013) for the comparisons with surface ozone.

4.3 AQUM NO_x emissions sensitivity experiments

We hypothesise that significant summer Run C–OMI positive biases in northern England and Scotland (Fig. 5) are caused by the AQUM's representation of point source (mainly power station) NO_x emissions. Therefore, to better understand these biases, we investigate sensitivity experiments of NO_x emissions (Table 2) for June–July–August (JJA) 2006 (Fig. 7a shows JJA Run C–OMI positive biases). Figure 7b–d shows the JJA AQUM NO_x emissions for runs C and E1 (with point sources removed) and their difference. The peak Run C NO_x emissions are around $1.8 \times 10^{-9} \text{ kg m}^{-2} \text{ s}^{-1}$. However, with point sources removed, the differences are $1.8 \times 10^{-9} \text{ kg m}^{-2} \text{ s}^{-1}$ in point source locations, showing that they make up a significant part of the emissions budget.

Figure 8a and b highlights the impact of removing point sources as column NO₂ over northern England reduces from $15\text{--}25 \times 10^{15} \text{ molecules cm}^{-2}$ to $4\text{--}5 \times 10^{15} \text{ molecules cm}^{-2}$. The Run E1–OMI MB now ranges between -10 and $-6 \times 10^{15} \text{ molecules cm}^{-2}$, while the Run C–OMI MB (Fig. 7a) is around $6\text{--}10 \times 10^{15} \text{ molecules cm}^{-2}$. Therefore, the switch in sign of the biases, of similar magnitude, indicates that the point source emissions play a significant role in the AQUM column NO₂ budget.

Run E2 aimed to test whether the point sources were responsible for the positive biases in Fig. 7a by using an idealised tracer of the power station emissions. Figure 8c shows the JJA tracer column with the OMI AKs applied, where peak columns range around $16\text{--}20 \times 10^{15} \text{ molecules cm}^{-2}$ over northern England. The minimum tracer values of $0 \times 10^{15} \text{ molecules cm}^{-2}$ are over the sea and continental Europe as there is no emission of the tracer there. Inspection of Figs. 7a and 8c suggest that the peak tracer columns overlap with the large Run C–OMI positive biases.

To test this more quantitatively, the spatial correlation between these peak concentrations from Run E2 were compared against a random tracer-MB (Run C) correlation distribution. The largest 100 tracer column pixels in Fig. 8c were compared against the MBs over the same locations in Fig. 7a, yielding a correlation of 0.45. Then, using a Monte-Carlo ap-

proach, a random 100 sample of the Fig. 7a land-based MB pixels (we use land bias pixels only as the biases in Fig. 7a are over land) were correlated against the largest 100 tracer sample. This was repeated 1000 times and then sorted from lowest to highest. The 5th and 95th percentiles were calculated at -0.162 and 0.158 , respectively. Our theory is that if the point sources are responsible for the peak Run C–OMI biases, then the peak tracer concentrations, which represent the point source emissions, should be in the same location as the peak biases. By looking at the random samples correlation, we see how the tracer-MB peak value concentration compares with randomly sampled MB locations. Since 0.45 is above the 95th percentile, this shows the tracer-MB peak correlation value is significant (is actually the greatest correlation – see Fig. 8d) and that AQUM's representation of point source emissions is linked to the AQUM overestimation of column NO_2 in northern England and Scotland.

4.4 Sensitivity to heterogeneous removal of N_2O_5

Figure 9 shows the winter and summer MBs between AQUM (with LBCs from GEMS) and OMI when heterogeneous hydrolysis of N_2O_5 is implemented in the model with $\gamma = 0.001$ (Run $\text{N}_2\text{O}_5\text{Low}$) and $\gamma = 0.02$ (Run $\text{N}_2\text{O}_5\text{High}$). In the Run C summer case (see Fig. 5a) there are positive northern England and Scotland biases of around $5\text{--}10 \times 10^{15} \text{ molecules cm}^{-2}$. We have shown that these positive biases are likely linked to AQUM's representation of point source emissions. However, by introducing N_2O_5 heterogeneous chemistry these positive biases are significantly reduced. In Run $\text{N}_2\text{O}_5\text{Low}$ (Fig. 9a) there is some impact on the biases as RMSE (over UK domain 8°W – 2°E and $50\text{--}60^\circ \text{N}$) decreases from 3.68×10^{15} to $3.39 \times 10^{15} \text{ molecules cm}^{-2}$ and FGE (over UK domain 8°W – 2°E and $50\text{--}60^\circ \text{N}$) also reduces very slightly. In Run $\text{N}_2\text{O}_5\text{High}$ (Fig. 9c) many of the positive biases over point sources are now insignificant and the RMSE decreases to $3.08 \times 10^{15} \text{ molecules cm}^{-2}$. However, over parts of continental Europe the intensity and spread of negative biases has increased, thus suggesting that $\gamma = 0.02$ might be too strong an uptake here. The FGE does go up slightly to 0.67 and we suspect that this is due to the introduction of negative biases over relatively clean or moderately polluted areas (e.g.

the Irish Sea and parts of the continent). Note that the correction of errors of large magnitude (e.g. over point sources) reduces RMSE because this metric penalises the large deviations between the model and the satellite-retrieved columns, while the introduction of errors of low magnitude over less polluted areas might increase the normalised errors given by FGE. The changes at the point source locations are most significant because of the large emissions of NO_x and aerosols suitable for this heterogeneous process to take place. Therefore, we suggest that while AQUM's representation of point sources may be responsible for the summer northern England/Scotland positive biases, including N_2O_5 heterogeneous chemistry with $\gamma = 0.02$ will partially account for this. In winter, the positive biases seen in Fig. 5b, $2\text{--}5 \times 10^{15} \text{ molecules cm}^{-2}$, decrease as γ increases, similarly as found for summer. In Run $\text{N}_2\text{O}_5\text{Low}$ (Fig. 9b) the spatial spread of significantly positive biases is only partially reduced, resulting in small decreases of RMSE (from 5.12×10^{15} to $5.05 \times 10^{15} \text{ molecules cm}^{-2}$) and FGE (from 0.63 to 0.62). For Run $\text{N}_2\text{O}_5\text{High}$ (Fig. 9d) the cluster of significantly positive biases has decreased spatially yielding the best comparisons, with RMSE and FGE values of $4.48 \times 10^{15} \text{ molecules cm}^{-2}$ and 0.60, respectively.

5 Conclusions

We have successfully used OMI satellite observations of column NO_2 over the UK to further explore the AQUM performance, extending on previous validation of the model which had only used surface data. In order to do this we have looked in detail at the satellite errors (random, systematic and smoothing) and derived an algorithm which reduces the retrieval random error component when averaging retrievals. This allows more critical AQUM-satellite comparisons as the time average random error component can be reduced by 30–70 % in all seasons.

Based on the summer and winter comparisons, the standard (operational) AQUM overestimates column NO_2 over northern England/Scotland by $5\text{--}10 \times 10^{15} \text{ molecules cm}^{-2}$ and over the northern domain by $2\text{--}5 \times 10^{15} \text{ molecules cm}^{-2}$. The use of a different set of lateral boundary conditions (from the MACC reanalysis), which are known to increase AQUM's sur-

face ozone positive bias (Savage et al., 2013), also increases the error in the NO_2 columns. The AQUM column NO_2 is increased, especially in winter, by $2\text{--}5 \times 10^{15}$ molecules cm^{-2} , resulting in poorer comparisons with OMI.

From multiple sensitivity experiments on the UK NO_x point source emissions we conclude that it was AQUM's representation of these emissions which very likely caused the northern England/Scotland summer biases. By emitting an idealised tracer in the NO_x points sources we found a significant correlation of the peak tracer columns to the AQUM – OMI MBs. Finally, introducing N_2O_5 heterogeneous chemistry in AQUM improves the AQUM–OMI comparisons in both seasons. In winter, the spatial extent of positive biases, $2\text{--}5 \times 10^{15}$ molecules cm^{-2} , decreases. In summer, the northern England biases decrease both spatially and in magnitude from $5\text{--}10$ to $0\text{--}5 \times 10^{15}$ molecules cm^{-2} . Therefore, this suggests that in summer the AQUM's representation of NO_x point sources is inaccurate but can be partially masked by the introduction of N_2O_5 heterogeneous chemistry.

As this study has shown the potential use of satellite observations, along with the time-averaged random error algorithm, to evaluate AQUM, the data could be used in future to evaluate operational air quality forecasts. We also show that the heterogeneous loss of N_2O_5 on aerosol is an important sink of NO_2 and should be included in the operational AQUM.

Appendix A

The equations for mean bias (MB), root mean square error (RMSE), modified normalised mean bias (MNMB) and the fractional gross error (FGE) are given here, where f is the model output, o is the satellite measurements, N is the total number of elements and i is the index.

Mean Bias (MB):

$$\text{MB} = \frac{1}{N} \sum_i (f_i - o_i) \quad (\text{A1})$$

Modified Normalised Mean Bias (MNMB):

$$\text{MNMB} = \frac{2}{N} \sum \frac{(f_i - o_i)}{f_i + o_i} \quad (\text{A2})$$

Root Mean Square Error (RMSE):

$$\text{RMSE} = \sqrt{\frac{1}{N} \sum_i (f_i - o_i)^2} \quad (\text{A3})$$

5 Fractional Gross Error (FGE):

$$\text{FGE} = \frac{2}{N} \sum_i \left| \frac{f_i - o_i}{f_i + o_i} \right| \quad (\text{A4})$$

Acknowledgements. We acknowledge the use of the Tropospheric Emissions Monitoring Internet Service (TEMIS) OMI dataset used in this study. This work was supported by the UK Natural Environment Research Council (NERC) and National Centre for Earth Observation (NCEO). Richard Pope thanks the NCEO for a Ph.D. studentship to undertake this work. We are grateful to Ben Johnson at the Met Office who provided advice for the implementation of aerosol growth and surface area diagnostics in CLASSIC.

References

- Bellouin, N., Rae, J., Jones, A., Johnson, C., Haywood, J., and Boucher, O.: Aerosol forcing in the Climate Model Intercomparison Project (CMIP5) simulations by HadGEM2-ES and the role of ammonium nitrate, *J. Geophys. Res.-Atmos.*, 116, D20206, doi:10.1029/2011JD016074, 2011.
- 15 Belmonte Rivas, M., Veefkind, P., Boersma, F., Levelt, P., Eskes, H., and Gille, J.: Intercomparison of daytime stratospheric NO₂ satellite retrievals and model simulations, *Atmospheric Measurement Techniques Discussions*, 7, 895–948, doi:10.5194/amtd-7-895-2014, <http://www.atmos-meas-tech-discuss.net/7/895/2014/>, 2014.

Blond, N., Boersma, K. F., Eskes, H. J., van der A, R. J., Van Roozendael, M., De Smedt, I., Bergametti, G., and Vautard, R.: Intercomparison of SCIAMACHY nitrogen dioxide observations, in situ measurements and air quality modeling results over Western Europe, *J. Geophys. Res.-Atmos.*, 112, D10311, doi:10.1029/2006JD007277, 2007.

5 Boersma, K., Eskes, H., and Brinksma, E.: Error analysis for tropospheric NO₂ retrieval from space, *J. Geophys. Res.-Atmos.*, 109, D04311, doi:10.1029/2003JD003962, 2004.

Boersma, K. F., Eskes, H. J., Veefkind, J. P., Brinksma, E. J., van der A, R. J., Sneep, M., van den Oord, G. H. J., Levelt, P. F., Stammes, P., Gleason, J. F., and Bucsela, E. J.: Near-real time retrieval of tropospheric NO₂ from OMI, *Atmos. Chem. Phys.*, 7, 2103–2118, doi:10.5194/acp-7-2103-2007, 2007.

10 Boersma, K., Jacob, D., Bucsela, E., Perring, A., Dirksen, R., van der A, R., Yantosca, R., Park, R., Wenig, M., Bertram, T., and Cohen, R.: Validation of {OMI} tropospheric {NO₂} observations during INTEX-B and application to constrain emissions over the eastern United States and Mexico, *Atmos. Environ.*, 42, 4480–4497, doi:10.1016/j.atmosenv.2008.02.004, 2008.

15 Boersma, K. F., Jacob, D. J., Trainic, M., Rudich, Y., DeSmedt, I., Dirksen, R., and Eskes, H. J.: Validation of urban NO₂ concentrations and their diurnal and seasonal variations observed from the SCIAMACHY and OMI sensors using in situ surface measurements in Israeli cities, *Atmos. Chem. Phys.*, 9, 3867–3879, doi:10.5194/acp-9-3867-2009, 2009.

20 Boersma, K., Braak, R., and van der A, R.: Dutch OMI NO₂ (DOMINO) data product v2.0, Tropospheric Emissions Monitoring Internet Service on-line Documentation, available at: http://www.temis.nl/docs/OMI_NO2_HE5_2.0_2011.pdf (last access: June 2014), KNMI, the Netherlands, 2011a.

Boersma, K. F., Eskes, H. J., Dirksen, R. J., van der A, R. J., Veefkind, J. P., Stammes, P., Huijnen, V., Kleipool, Q. L., Sneep, M., Claas, J., Leitão, J., Richter, A., Zhou, Y., and Brunner, D.: An improved tropospheric NO₂ column retrieval algorithm for the Ozone Monitoring Instrument, *Atmos. Meas. Tech.*, 4, 1905–1928, doi:10.5194/amt-4-1905-2011, 2011b.

25 Braak, R.: Row Anomaly Flagging Rules Lookup Table, KNMI Technical Document TN-OMIE-KNMI-950, KNMI, the Netherlands, 2010.

Curier, R., Kranenburg, R., Segers, A., Timmermans, R., and Schaap, M.: Synergistic use of {OMI} {NO₂} tropospheric columns and LOTOS-EUROS to evaluate the {NO_x} emission trends across Europe, *Remote Sens. Environ.*, 149, 58–69, doi:10.1016/j.rse.2014.03.032, 2014.

30 DEFRA: Automatic Urban and Rural Network (AURN), available at: <http://uk-air.defra.gov.uk/networks/network-info?view=aurn> (last access: 2014), DEFRA, UK, 2012.

- Dirksen, R. J., Boersma, K. F., Eskes, H. J., Ionov, D. V., Bucsela, E. J., Levelt, P. F., and Kelder, H. M.: Evaluation of stratospheric NO₂ retrieved from the Ozone Monitoring Instrument: Inter-comparison, diurnal cycle, and trending, *Journal of Geophysical Research: Atmospheres*, 116, n/a–n/a, doi:10.1029/2010JD014943, <http://dx.doi.org/10.1029/2010JD014943>, 2011.
- 5 Eskes, H. J. and Boersma, K. F.: Averaging kernels for DOAS total-column satellite retrievals, *Atmos. Chem. Phys.*, 3, 1285–1291, doi:10.5194/acp-3-1285-2003, 2003.
- Fitzgerald, J. W.: Approximation formulas for the equilibrium size of an aerosol particle as a function of its dry size and composition and the ambient relative humidity, *J. Appl. Meteorol.*, 14, 1044–1049, 1975.
- 10 Foley, K. M., Roselle, S. J., Appel, K. W., Bhawe, P. V., Pleim, J. E., Otte, T. L., Mathur, R., Sarwar, G., Young, J. O., Gilliam, R. C., Nolte, C. G., Kelly, J. T., Gilliland, A. B., and Bash, J. O.: Incremental testing of the Community Multiscale Air Quality (CMAQ) modeling system version 4.7, *Geosci. Model Dev.*, 3, 205–226, doi:10.5194/gmd-3-205-2010, 2010.
- Han, K., Lee, C., Lee, J., Kim, J., and Song, C.: A comparison study between model-predicted and
- 15 OMI-retrieved tropospheric NO₂ columns over the Korean peninsula, *Atmos. Environ.*, 45, 2962–2971, 2011.
- HoC: House of Commons Environmental Audit Report (HCEA): Air Quality: Vol 1 (2009–2010), available at: <http://www.publications.parliament.uk/pa/cm200910/cmselect/cmenvaud/229/229i.pdf> (last access: February 2014), House of Commons, London, UK, 2010.
- 20 Hollaway, M. J., Arnold, S. R., Challinor, A. J., and Emberson, L. D.: Intercontinental trans-boundary contributions to ozone-induced crop yield losses in the Northern Hemisphere, *Biogeosciences*, 9, 271–292, doi:10.5194/bg-9-271-2012, 2012.
- Hollingsworth, A., Engelen, R., Benedetti, A., Dethof, A., Flemming, J., Kaiser, J., Morcrette, J., Simmons, A., Textor, C., Boucher, O., Chevallier, F., Rayner, P., Elbern, H., Eskes, H., Granier, C., Peuch, V.-H., Rouil, L., and Schultz, M. G.: Toward a monitoring and forecasting system for atmospheric composition: the GEMS project, *B. Am. Meteorol. Soc.*, 89, 1147–1164, 2008.
- 25 Huijnen, V., Eskes, H. J., Poupkou, A., Elbern, H., Boersma, K. F., Foret, G., Sofiev, M., Valdebenito, A., Flemming, J., Stein, O., Gross, A., Robertson, L., D'Isidoro, M., Kioutsioukis, I., Friese, E., Amstrup, B., Bergstrom, R., Strunk, A., Vira, J., Zyryanov, D., Maurizi, A., Melas, D., Peuch, V.-H., and Zerefos, C.: Comparison of OMI NO₂ tropospheric columns with an ensemble of global and
- 30 European regional air quality models, *Atmos. Chem. Phys.*, 10, 3273–3296, doi:10.5194/acp-10-3273-2010, 2010.

- Inness, A., Baier, F., Benedetti, A., Bouarar, I., Chabrillat, S., Clark, H., Clerbaux, C., Coheur, P., Engelen, R. J., Errera, Q., Flemming, J., George, M., Granier, C., Hadji-Lazaro, J., Huijnen, V., Hurtmans, D., Jones, L., Kaiser, J. W., Kapsomenakis, J., Lefever, K., Leitão, J., Razinger, M., Richter, A., Schultz, M. G., Simmons, A. J., Suttie, M., Stein, O., Thépaut, J.-N., Thouret, V., Vrekoussis, M., Zerefos, C., and the MACC team: The MACC reanalysis: an 8 yr data set of atmospheric composition, *Atmos. Chem. Phys.*, 13, 4073–4109, doi:10.5194/acp-13-4073-2013, 2013.
- Irie, H., Boersma, K., Kanaya, Y., Takashima, H., Pan, X., and Wang, Z.: Quantitative bias estimates for tropospheric NO₂ columns retrieved from SCIAMACHY, OMI, and GOME-2 using a common standard for East Asia, *Atmospheric Measurement Techniques*, 5, 2403–2411, 2012.
- Lauer, A., Dameris, M., Richter, A., and Burrows, J. P.: Tropospheric NO₂ columns: a comparison between model and retrieved data from GOME measurements, *Atmos. Chem. Phys.*, 2, 67–78, doi:10.5194/acp-2-67-2002, 2002.
- Macintyre, H. L. and Evans, M. J.: Sensitivity of a global model to the uptake of N₂O₅ by tropospheric aerosol, *Atmos. Chem. Phys.*, 10, 7409–7414, doi:10.5194/acp-10-7409-2010, 2010.
- Magi, B. I. and Hobbs, P. V.: Effects of humidity on aerosols in southern Africa during the biomass burning season, *J. Geophys. Res.-Atmos.*, 108, 8495, doi:10.1029/2002JD002144, 2003.
- Monks, S., Arnold, S., and Chipperfield, M.: Evidence for El Niño–Southern Oscillation (ENSO) influence on Arctic CO interannual variability through biomass burning emissions, *Geophys. Res. Lett.*, 39, L14804, doi:10.1029/2012GL052512, 2012.
- O'Connor, F. M., Johnson, C. E., Morgenstern, O., Abraham, N. L., Braesicke, P., Dalvi, M., Folberth, G. A., Sanderson, M. G., Telford, P. J., Voulgarakis, A., Young, P. J., Zeng, G., Collins, W. J., and Pyle, J. A.: Evaluation of the new UKCA climate-composition model – Part 2: The Troposphere, *Geosci. Model Dev.*, 7, 41–91, doi:10.5194/gmd-7-41-2014, 2014.
- Pope, R., Savage, N., Chipperfield, M., Arnold, S., and Osborn, T.: The influence of synoptic weather regimes on UK air quality: analysis of satellite column NO₂, *Atmos. Sci. Lett.*, 15, 211–217, doi:10.1002/asl2.492, 2014.
- Poupkou, A., Giannaros, T., Markakis, K., Kioutsoukis, I., Curci, G., Melas, D., and Zerefos, C.: A model for European Biogenic Volatile Organic Compound emissions: Software development and first validation, *Environmental Modelling & Software*, 25, 1845 – 1856, doi:http://dx.doi.org/10.1016/j.envsoft.2010.05.004, http://www.sciencedirect.com/science/article/pii/S1364815210001441, 2010.

- Randerson, J., Kasibhatla, P., Kasischke, E., Hyer, E., Giglio, L., Collatz, G., and van der Werf, G.: Global fire emissions database (GFED), version 1, <http://daac.ornl.gov> (last access: 2 October 2012), 2005.
- 5 Savage, N. H., Pyle, J. A., Braesicke, P., Wittrock, F., Richter, A., Nüß, H., Burrows, J. P., Schultz, M. G., Pulles, T., and van Het Bolscher, M.: The sensitivity of Western European NO₂ columns to interannual variability of meteorology and emissions: a model – GOME study, *Atmos. Sci. Lett.*, 9, 182–188, 2008.
- 10 Savage, N. H., Agnew, P., Davis, L. S., Ordóñez, C., Thorpe, R., Johnson, C. E., O'Connor, F. M., and Dalvi, M.: Air quality modelling using the Met Office Unified Model (AQUM OS24-26): model description and initial evaluation, *Geosci. Model Dev.*, 6, 353–372, doi:10.5194/gmd-6-353-2013, 2013.
- 15 Seigneur, C., Pun, B., Pai, P., Louis, J.-F., Solomon, P., Emery, C., Morris, R., Zahniser, M., Worsnop, D., Koutrakis, P., White, W., and Tombach, I.: Guidance for the performance evaluation of three-dimensional air quality modeling systems for particulate matter and visibility, *J. Air Waste Manage.*, 50, 588–599, 2000.
- Steinbacher, M., Zellweger, C., Schwarzenbach, B., Bugmann, S., Buchmann, B., Ordonez, C., Prevot, A., and Hueglin, C.: Nitrogen oxide measurements at rural sites in Switzerland: bias of conventional measurement techniques, *J. Geophys. Res.-Atmos.*, 112, D11307, doi:10.1029/2006JD007971, 2007.
- 20 Tie, X., Emmons, L., Horowitz, L., Brasseur, G., Ridley, B., Atlas, E., Stround, C., Hess, P., Klonnecki, A., Madronich, S., Talbot, R., and Dibb, J.: Effect of sulfate aerosol on tropospheric NO_x and ozone budgets: model simulations and TOPSE evidence, *J. Geophys. Res.-Atmos.*, 108, 2156–2202, doi:10.1029/2001JD001508, 2003.
- 25 van Noije, T. P. C., Eskes, H. J., Dentener, F. J., Stevenson, D. S., Ellingsen, K., Schultz, M. G., Wild, O., Amann, M., Atherton, C. S., Bergmann, D. J., Bey, I., Boersma, K. F., Butler, T., Cofala, J., Drevet, J., Fiore, A. M., Gauss, M., Hauglustaine, D. A., Horowitz, L. W., Isaksen, I. S. A., Krol, M. C., Lamarque, J.-F., Lawrence, M. G., Martin, R. V., Montanaro, V., Müller, J.-F., Pitari, G., Prather, M. J., Pyle, J. A., Richter, A., Rodriguez, J. M., Savage, N. H., Strahan, S. E., Sudo, K., Szopa, S., and van Roozendaal, M.: Multi-model ensemble simulations of tropospheric NO₂ compared with GOME retrievals for the year 2000, *Atmos. Chem. Phys.*, 6, 2943–2979, doi:10.5194/acp-6-2943-2006, 2006.
- 30 van der A, R. J., Eskes, H. J., Boersma, K. F., van Noije, T. P. C., Van Roozendaal, M., De Smedt, I., Peters, D. H. M. U., and Meijer, E. W.: Trends, seasonal variability and dominant NO_x source de-

rived from a ten year record of NO₂ measured from space, *Journal of Geophysical Research: Atmospheres*, 113, n/a–n/a, doi:10.1029/2007JD009021, <http://dx.doi.org/10.1029/2007JD009021>, 2008.

5 Varutbangkul, V., Brechtel, F. J., Bahreini, R., Ng, N. L., Keywood, M. D., Kroll, J. H., Flagan, R. C., Seinfeld, J. H., Lee, A., and Goldstein, A. H.: Hygroscopicity of secondary organic aerosols formed by oxidation of cycloalkenes, monoterpenes, sesquiterpenes, and related compounds, *Atmos. Chem. Phys.*, 6, 2367–2388, doi:10.5194/acp-6-2367-2006, 2006.

10 Velders, G. J., Granier, C., Portmann, R. W., Pfeilsticker, K., Wenig, M., Wagner, T., Platt, U., Richter, A., and Burrows, J. P.: Global tropospheric NO₂ column distributions: comparing three-dimensional model calculations with GOME measurements, *J. Geophys. Res.-Atmos.*, 106, 12643–12660, 2001.

Visschedijk, A., Zanveld, P., and van der Gon, H.: A high resolution gridded European emission database for the EU integrated project GEMS, TNO report 2007-A-R0233/B, 2007.

15 WHO: Air Quality and Health, available at: <http://www.who.int/mediacentre/factsheets/fs313/en/> (last access: February 2014), World Health Organisation, Geneva, Switzerland, 2011.

Table 1. The average column NO₂, column NO₂ error and column NO₂ error as calculated in Sect. 2.2 for multiple locations across Europe in summer and winter ($\times 10^{15}$ molecules/cm²).

Place	Column NO ₂		Column NO ₂ Error		Error (Sect. 2.2)	
	Summer	Winter	Summer	Winter	Summer	Winter
London 1°W-1°E, 51-51.5°N	9.86	10.7	9.68	9.13	4.24	4.52
Benelux 3-7°E, 50.5-52.5°N	9.57	11.4	7.09	9.24	3.98	4.82
Po Valley 7-9°E, 44.25-45.5°N	3.35	11.9	2.44	9.88	1.42	4.66
Northern England 3-0°W, 52.5-54°N	8.11	8.06	7.13	6.56	3.47	3.42
North Sea 0-8°E, 54-60°N	1.48	2.22	1.94	2.12	0.86	1.01
Scandinavia 6-16°E, 54-63°N	1.48	2.10	1.49	2.12	0.74	1.16

Table 2. List of AQUM runs and experiments.

Run ID	Run Description
C	Control run (GEMS LBCs)
MACC	MACC LBCs
E1	No point sources emissions
E2	Idealised point source tracer
N ₂ O ₅ Low	With N ₂ O ₅ heterogeneous chemistry with $\gamma = 0.001$
N ₂ O ₅ High	As run N ₂ O ₅ Low but with $\gamma = 0.02$

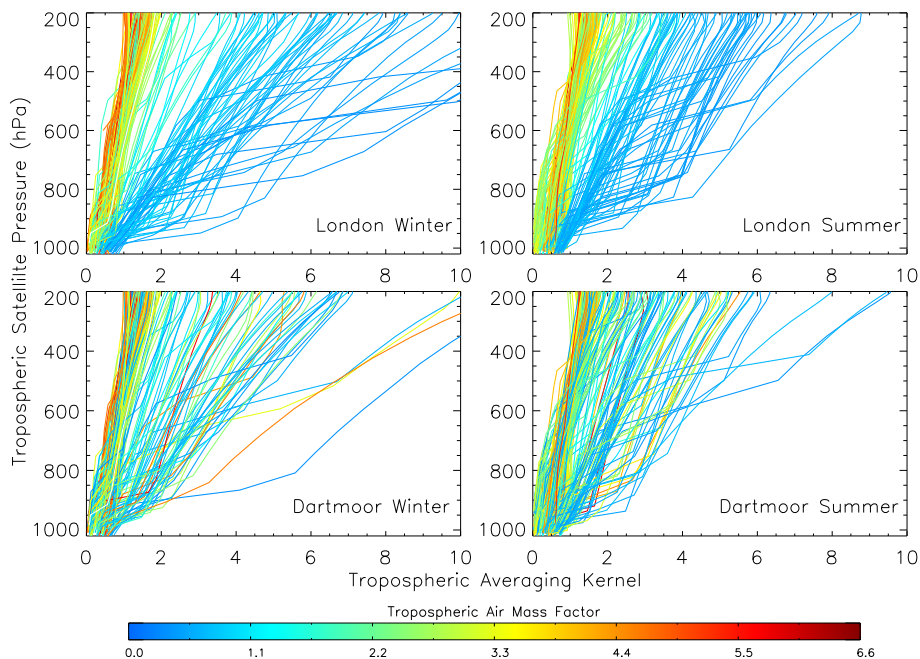


Figure 1. Example OMI averaging kernels for London (top) and Dartmoor (bottom) for summer (right) and winter (left) 2006. Averaging kernels have been coloured according to their respective tropospheric air mass factor values.

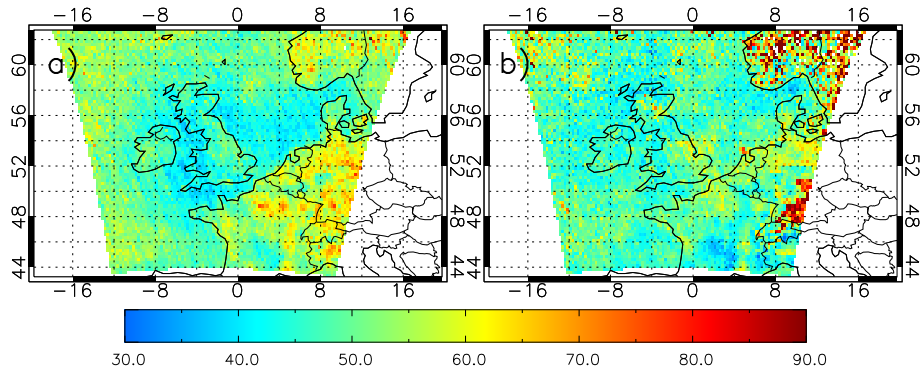


Figure 2. New seasonal satellite mean error, obtained by reduction of random error using the methodology described in Sect. 2, as a percentage of simple seasonal mean of satellite total error for 2006. Smoothing errors have been removed. **(a)** Summer and **(b)** winter.

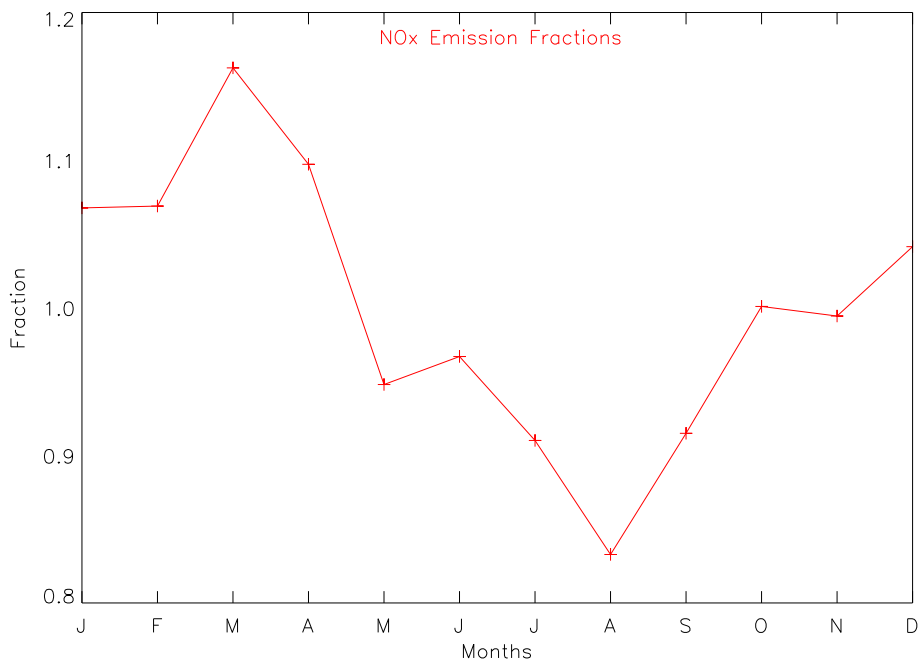


Figure 3. NO_x emissions seasonal cycle, based on Visschedijk et al. (2007), which is applied to AQUM's NO_x emission annual totals.

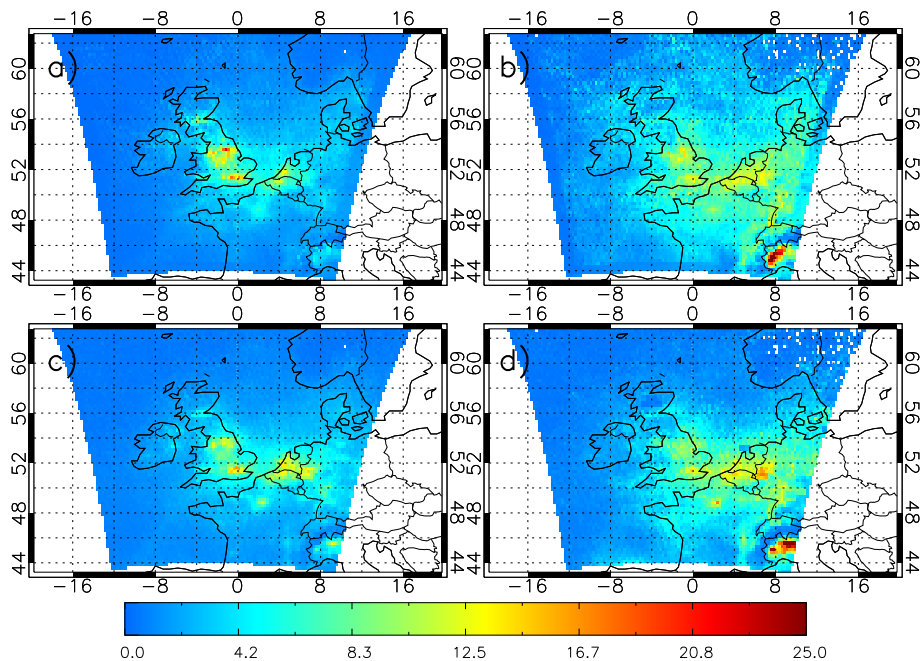


Figure 4. Tropospheric NO_2 column ($\times 10^{15}$ molecules cm^{-2}), 2006, for (a) AQUM Run C (with averaging kernels (AK) applied) summer, (b) AQUM Run C (AKs applied) winter, (c) OMI summer and (d) OMI winter.

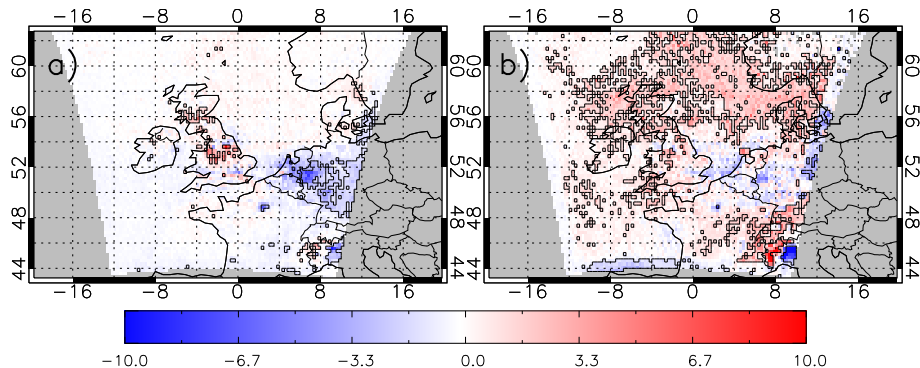


Figure 5. Mean bias in tropospheric NO₂ column ($\times 10^{15}$ molecules cm⁻²), 2006, between AQUUM Run C (AKs applied) and OMI for (a) summer (RMSE = 3.68×10^{15} molecules cm⁻² and FGE = 0.65) and (b) winter (RMSE = 5.12×10^{15} molecules cm⁻² and FGE = 0.63). The RMSE and FGE are over the UK between 8° W–2° E and 50–60° N and black polygoned regions show significant differences. Also the same for mean bias plots in Figs. 6–9.

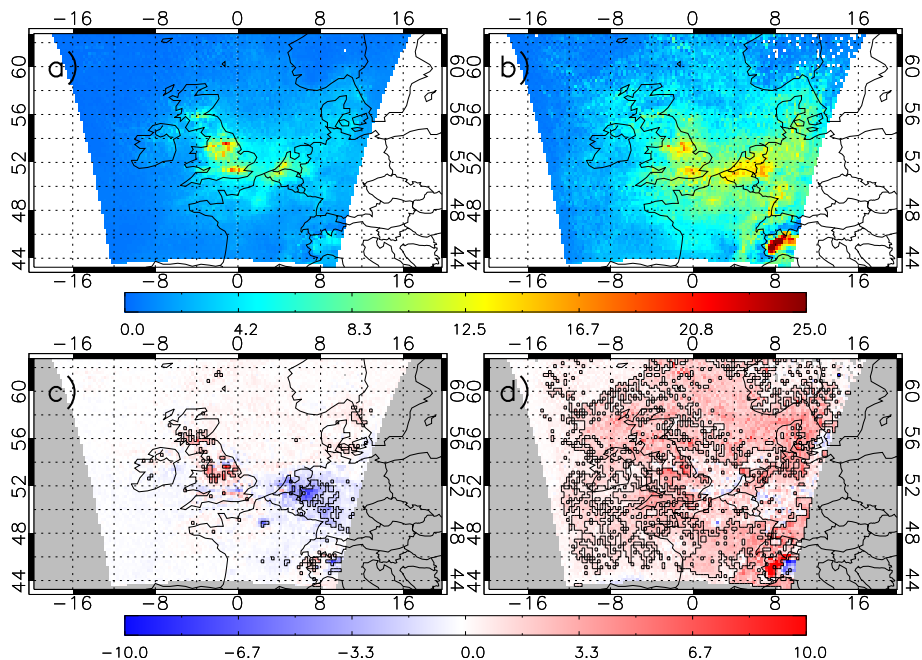


Figure 6. Tropospheric NO₂ column ($\times 10^{15}$ molecules cm⁻²), 2006, from AQUM Run MACC (AKs applied) for (a) summer and (b) winter. AQUM Run MACC (AKs applied) and OMI mean bias for (c) summer (RMSE = 3.74×10^{15} molecules cm⁻² and FGE = 0.63) and (d) winter (RMSE = 6.00×10^{15} molecules cm⁻² and FGE = 0.65).

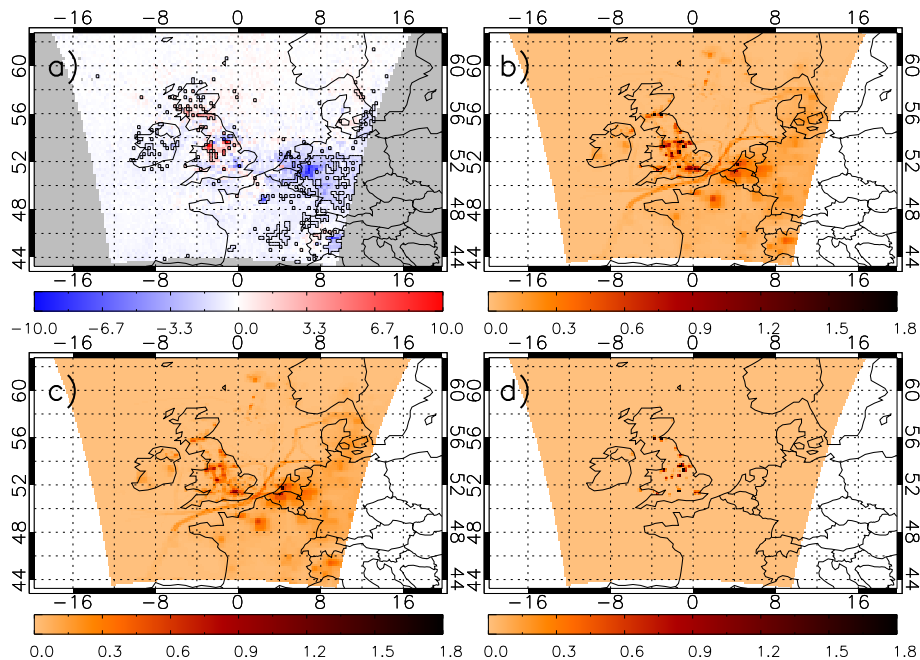


Figure 7. AQUM Run C (AKs applied)–OMI tropospheric NO₂ column ($\times 10^{15}$ molecules cm⁻²) JJA 2006 mean bias. These are the control MBs to compare to the point source sensitivity experiments (RMSE = 3.64×10^{15} molecules cm⁻² and FGE = 0.66). NO_x emissions ($\times 10^{-9}$ kg m⁻² s⁻¹), JJA 2006, used in AQUM for (b) Run C and (c) Run E1. (d) shows the difference between (b) and (c).

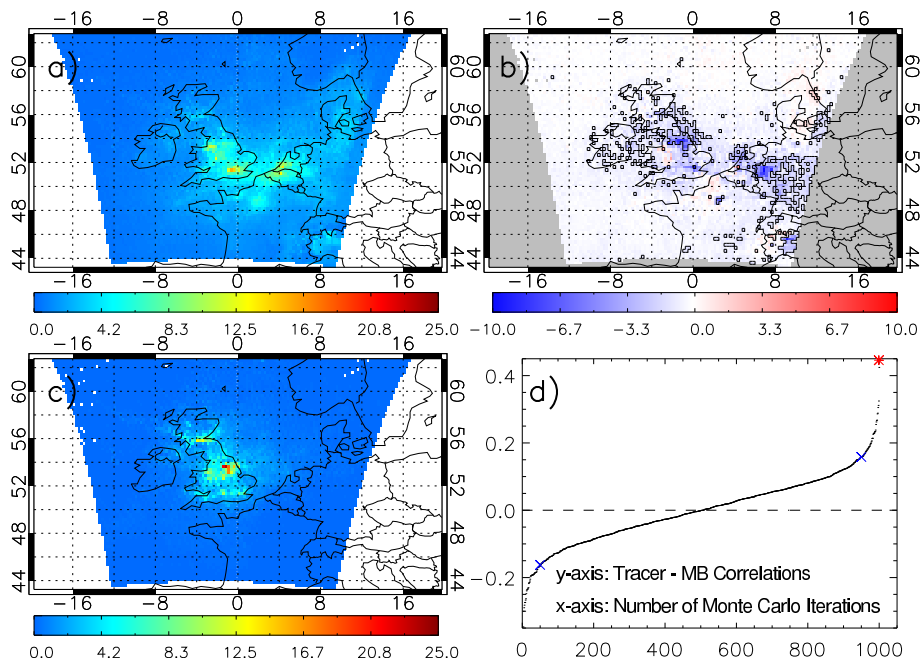


Figure 8. Tropospheric column ($\times 10^{15}$ molecules cm^{-2}), JJA 2006, for (a) AQUM Run E1 NO_2 (AKs applied), (b) AQUM Run E1 NO_2 (AKs applied)–OMI (RMSE = 3.02×10^{15} molecules cm^{-2} and FGE = 0.68) and (c) AQUM Run E2 Tracer (AKs applied). (d) Peak Run E2 and co-located Run C–OMI MB correlation (red star) significance distribution. Black dots are Run E2 and random Run C–OMI MB correlations. Blue X = 5th and 95th percentiles of the 1000 size sample.

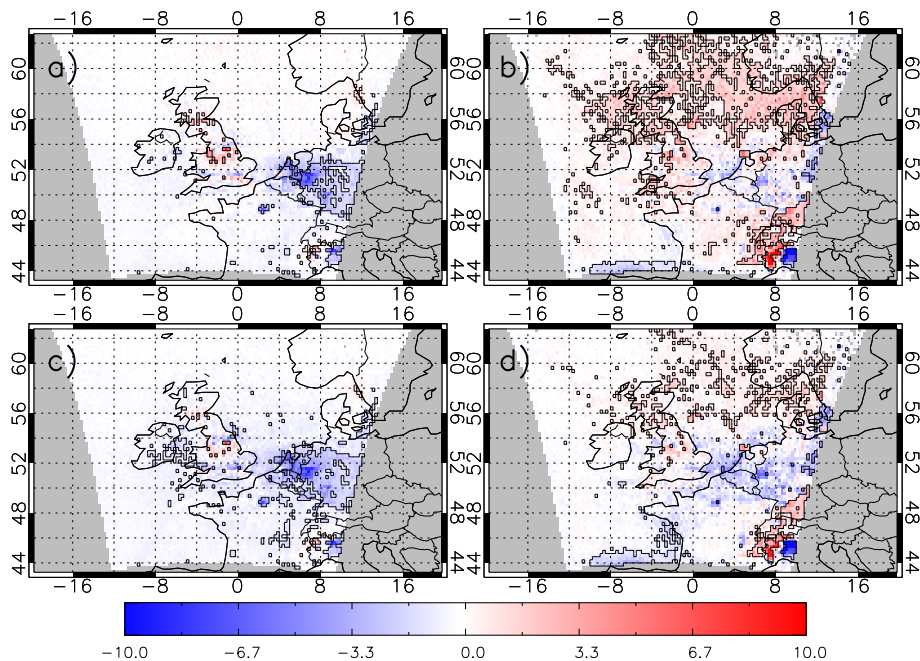


Figure 9. MB in tropospheric NO_2 column ($\times 10^{15}$ molecules cm^{-2}), 2006, between AQUM (AKs applied)–OMI for (a) summer $\gamma=0.001$ ($\text{RMSE}=3.39 \times 10^{15}$ molecules cm^{-2} and $\text{FGE}=0.65$), (b) winter $\gamma=0.001$ ($\text{RMSE}=5.05 \times 10^{15}$ molecules cm^{-2} and $\text{FGE}=0.62$), (c) summer $\gamma=0.02$ ($\text{RMSE}=3.08 \times 10^{15}$ molecules cm^{-2} and $\text{FGE}=0.67$) and (d) winter $\gamma=0.02$ ($\text{RMSE}=4.48 \times 10^{15}$ molecules cm^{-2} and $\text{FGE}=0.60$).